ACS SENSORS

pubs.acs.org/acssensors

Article

Chromo-Fluorogenic Rhodamine-Based Amphiphilic Probe as a Selective and Sensitive Sensor for Intracellular Cu(I) in Living Cells

Eunhye Jeong, Chang Hyeon Ha, Ashwani Kumar, Won Hur, Gi Hun Seong,* and Pil Seok Chae*

Cite This: *ACS Sens.* 2024, 9, 1419−1427

Read Online

ACCESS | Metrics & More | Article Recommendations | Supporting Information

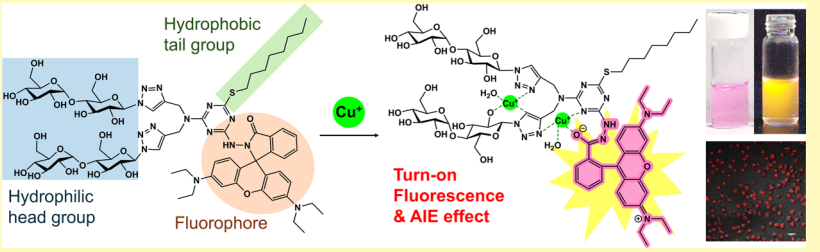

ABSTRACT: Fluorescent probes are widely studied for metal ion detection because of their multiple favorable properties such as high sensitivity and selectivity, quick response, naked eye detection, and in situ monitoring. However, optical probes that can effectively detect the Cu(I) level in cell interiors are rare due to the difficulty associated with selectively and sensitively detecting this metal ion in a cell environment. Therefore, we designed and synthesized three water-soluble probes (**1**−**3**) with a 1,3,5-triazine core decorated by three substituents: a hydrophobic alkyl chain, a hydrophilic maltose, and a rhodamine B hydrazine fluorophore. Among the probes, probe **1**, which has an octyl chain and a branched maltose group, was the most effective at sensing Cu^+ in aqueous solution. Upon addition of Cu^+, this probe showed a dramatic color change from colorless to pink in daylight and displayed an intense yellow fluorescence emission under 365 nm light. The limit of detection and dissociation constant (K_d) of this probe were 20 nM and 1.1×10^{-12} M, respectively, which are the lowest values reported to date. The two metal ion-binding sites and the aggregation-induced emission enhancement effect, endowed by the branched maltose group and the octyl chain, respectively, are responsible for the high sensitivity and selectivity of this probe for Cu^+ detection, as demonstrated by ^{1}H NMR, dynamic light scattering, and transmission electron microscopy studies. Furthermore, the probe successfully differentiated the Cu(I) level of cancer cells from that of the normal cells. Thus, the probe holds potential for real-time monitoring of Cu(I) level in biological samples and bioimaging of cancer cells.

KEYWORDS: *chromo-fluorogenic sensor, AIE, amphiphilic structure, Cu^+ sensing, 100 percentage aqueous media, live cell imaging*

Copper is used as a cofactor in a range of biological enzymes, including tyrosinase, cytochrome c oxidase, and superoxide dismutase.[1] Copper is vital for aerobic respiration, oxygen stress protection, and cell growth, as well as peptide hormone regulation and blood clotting factors in all eukaryotes.[2] Nonetheless, a high copper level inside cells can produce reactive oxygen species that have adverse effects on DNA, proteins, and lipids.[3−6] Moreover, abnormal levels of copper are implicated in various diseases. For example, Wilson disease and cancer have both been linked to copper accumulation, and Menkes disease results from copper deficiency.[7] Copper is also associated with neuronal diseases such as familial amyotrophic lateral sclerosis, Alzheimer's disease, and prion diseases with neuronal spongiform encephalopathy.[8,9] Thus, copper homeostasis is important to cell physiology and requires a delicate mechanism because copper is both essential and toxic to the human body.[10] In cytoplasm, the monovalent form of copper (Cu(I)) prevails in the protein-bound state because of reducing environments of cytoplasm.[11] Many kinds of cancer cells have abnormally high amounts of Cu^+ in their cytoplasm and serum to meet the growth rates of cancer cells, which are faster than those of normal cells.[12] Therefore, a Cu^+ chelator has been delivered together with a chemotherapeutic agent for cancer treatment.[13]

Fluorescence sensors are widely used to detect metal ions because fluorescence assays are fast, nondestructive, highly sensitive, and suitable for high-throughput screening applications.[14−16] Whereas most metal ions are soluble in water, many fluorescent molecules are water-insoluble and hydrophobic. Thus, an organic solvent is often required to detect a target analyte in environmental or biological samples. Recent studies have focused on developing water-soluble chemical sen-

Received: November 22, 2023
Revised: February 21, 2024
Accepted: February 23, 2024
Published: March 7, 2024

https://doi.org/10.1021/acssensors.3c02496
ACS Sens. 2024, 9, 1419−1427

sors.[17−19] Fluorescent dyes with aggregation-induced emission enhancement (AIE) have recently gained a lot of attention due to their ability to fluoresce when interacting with analytes.[20,21] Among many fluorophores, rhodamine B derivatives have favorable attributes, such as long emission wavelengths and high quantum yields. Rhodamine B is colorless in its spirolactam ring (closed) form, becomes pink, and fluoresces strongly when spirolactam ring opening is induced by analyte binding. As a result, many rhodamine B-based chemosensors have been developed to detect various metal ions, including Cu^{2+}, in living cells.[22−25] In contrast, only a few fluorescent probes can selectively detect Cu^{+} in biological samples.[26−35] To selectively detect Cu(I) levels in cell interiors, a chemical sensor first needs to penetrate the cell membrane and bind only Cu^{+} in the presence of various anions, cations, and biomolecules. In addition, the chemical probe must distinguish Cu^{+} from other copper species (Cu^{2+} and Cu^{0}). Furthermore, the use of visible light for probe excitation and strong metal ion binding are favorable characteristics of fluorescent probes for cellular Cu^{+} detection.[36,37] As an attempt to achieve these goals, we designed and prepared novel 1,3,5-triazine-based fluorescent chemosensors (**1**−**3**) with a rhodamine fluorophore. Among them, probe **1** was identified as a chemical sensor offering highly effective Cu^{+} sensing in aqueous solution via both a vivid color change detectable by the naked eye and strong fluorescence emission under visible light irradiation. The fluorescence-based limit of detection (LOD) and dissociation constant (K_d) of this probe was 20 nM and 1.1 × 10^{-12} M, respectively, the lowest values for Cu^{+} detection reported so far. The superiority of probe **1** in Cu^{+} detection, compared with probes **2** and **3**, resulted from the strong binding affinity to Cu^{+} and the AIE effect. Furthermore, we successfully applied probe **1** for differentiation of intracellular Cu(I) level between cancer and normal cells, indicating that this probe holds significant potential for Cu^{+} bioimaging and disease detection.

RESULTS AND DISCUSSION

Probe Design and Synthesis. Water-soluble fluorescent probes can be used for real-time monitoring of analytes in environmental and biological samples. In addition, amphiphilic molecules tend to form self-assemblies in aqueous solutions, which could play a favorable role in analyte sensing through AIE. Therefore, we incorporated maltose and an alkyl chain into fluorescent probes as the hydrophilic and lipophilic groups, respectively (Figure 1A). Based on its ability to fluoresce upon analyte binding and subsequent ring opening, rhodamine B was used as the fluorophore in our probe design.[22−25] The three moieties of probe, maltose, alkyl chain, and rhodamine B were joined together using a 1,3,5-triazine scaffold as the core structure, an ideal platform for attaching three different groups due to the differentiated reactivity of three attachment sites for substituent introduction. In addition, the multiple amine groups present in this aromatic core potentially act as metal-binding sites. Resultantly, we designed three fluorescent probes (**1**−**3**) with the same core unit and fluorophore (1,3,5-triazine and rhodamine B, respectively) but different hydrophilic or lipophilic groups (Figure 1B). Probes **1** and **2** contain a branched dimaltose group; however, the former contains a long octyl chain, and the latter has a short ethyl chain. The two triazole rings generated over the course of conjugating the branched dimaltose group to the triazine core are known to cooperatively bind Cu^{+} via the nitrogen/carbon

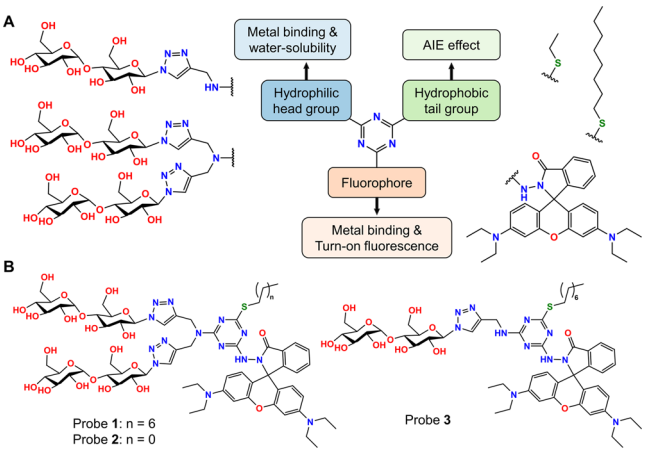

Figure 1. (A) Schematic representation of the building blocks used for probe preparation and their roles in metal ion sensing. The 1,3,5-triazine unit was used as a core structure in preparing all of the probes, and two different head and tail groups were attached to that core along with hydrazine-functionalized rhodamine B. An ethyl or octyl chain was attached to the triazine core as a lipophilic group via a thioether linkage, and one or two maltose groups were conjugated to the core via a triazole-containing amine linker. Rhodamine B was conjugated to the core ring as a fluorophore via a hydrazine linker. All probes share the triazine core and rhodamine B fluorophore, and they differ from one another in the number of hydrophilic groups and alkyl chain length. (B) Chemical structures of the new rhodamine B-based amphiphilic probes **1**−**3**.

atom.[38,39] Probes **1** and **3** both possess a long octyl chain, but probe **3** has an unbranched single maltose unit instead of a branched dimaltose group. The designed probes were prepared by a synthetic protocol comprising five steps and using 2,4,6-trichloro-1,3,5-triazine as the starting material (see Scheme S1).

Probe preparation started by attaching an alkyl chain (ethyl or octyl) to the triazine core via a thioether linkage. The resulting thioalkylated triazine derivatives (compounds **1a**/**2a**) were conjugated by hydrazine-functionalized rhodamine B to give disubstituted triazine rings (compounds **1b**/**2b**). To introduce two maltose units via an azide−alkyne cycloaddition reaction, two alkyne groups were conjugated to the triazine core by reacting compound **1b**/**2b** with dipropargylamine, which afforded bisalkyne-functionalized triazine derivatives (compounds **1c**/**2c**). Alternatively, compound **1b** was reacted with propargylamine to give the monoalkyne-functionalized triazine derivative (compound **3c**). The alkyne-functionalized triazine derivatives (**1c**/**2c**/**3c**) were then subjected to a click reaction with perbenzoylated maltosyl azide. Under Zemplén conditions using NaOMe, the resulting cycloaddition product underwent global deprotection to provide the three probes (**1**, **2**, and **3**) with different hydrophilic or lipophilic groups. The chemical structures of the probes were confirmed by ^{1}H and ^{13}C NMR spectroscopy and high-resolution mass spectrometry (see the Supporting Information).

Photophysical Properties of Probes 1−3 in the Absence and Presence of Metal Ions. When dissolved in water, probe **1** was colorless under daylight and showed blue luminescence under illumination of 365 nm (Figure S1). Probes **2** and **3** had little color in daylight or under UV irradiation. The UV−visible absorption spectra showed that only probe **1** in water had a weak absorption peak in the range of 400−500 nm, while the other probes showed no absorption

https://doi.org/10.1021/acssensors.3c02496
ACS Sens. 2024, 9, 1419−1427

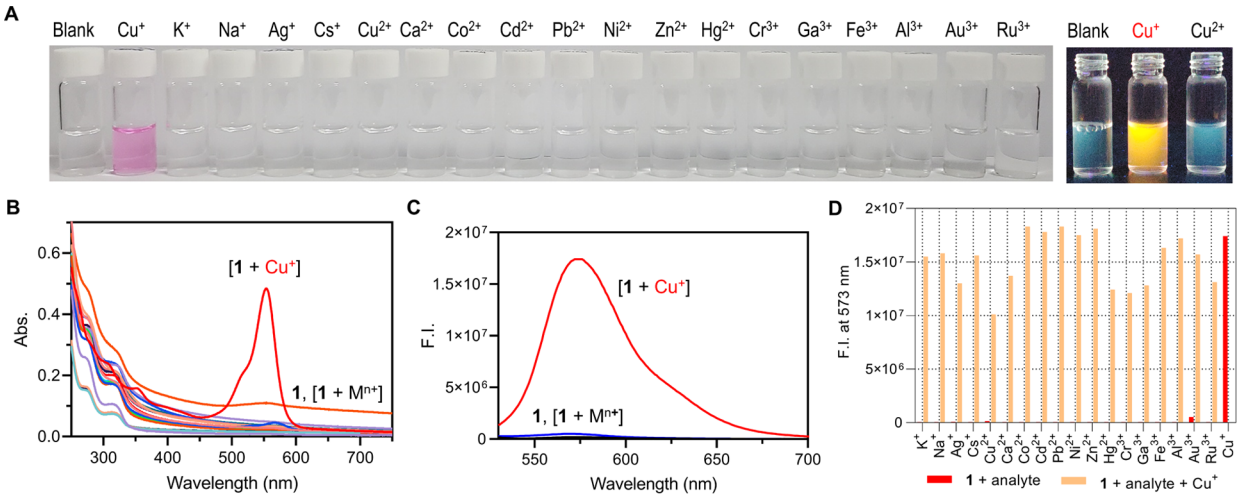

Figure 2. (A) A color image and fluorescence image of probe **1** solutions (10 μM) containing various metal ions (100 μM, 10 equiv) under irradiation of 365 nm. (B) UV/vis and (C) fluorescence spectra of those probe-metal ion solutions. Water was used as a solvent. (D) Interference study of probe **1** (10 μM) using different metal ions (100 μM) in the presence of Cu^{+} (100 μM).

of visible light (Figure S1B). In the fluorescence study, only probe **1** showed a strong fluorescence emission in the range of 400−550 nm upon excitation at 330 nm, which is responsible for its blue luminescence under UV irradiation (Figure S2A). Probes **2** and **3** had little fluorescence emission in the visible light region under the same conditions (Figures S2B and S2C).

Next, we investigated the metal ion sensing properties of these probes in water. Diverse metal ions (monovalent (K^{+}, Na^{+}, Ag^{+}, Cs^{+}, and Cu^{+}), divalent (Cu^{2+}, Ca^{2+}, Co^{2+}, Cd^{2+}, Pb^{2+}, Ni^{2+}, Zn^{2+}, and Hg^{2+}), and trivalent (Cr^{3+}, Ga^{3+}, Fe^{3+}, Al^{3+}, Au^{3+}, and Ru^{3+})) were included in this investigation. When Cu^{+} (100 μM) was added to an aqueous solution containing probe **2** (10 μM), the solution changed from colorless to pink, as detected by the naked eye in daylight (Figure S3A). The addition of Cu^{2+} or Hg^{2+} to the probe **2** solution produced a weak purple rather than a pink. Similar results were obtained for probe **3** (Figure S3B). The other metal ions failed to produce color changes in the probe solutions. Under illumination of 365 nm, the solutions containing probes **2** and **3** showed luminescent color changes from blue to orange and green, respectively, upon the addition of Cu^{+}. When added to the probe solutions, Hg^{2+} or Au^{3+} gave a weaker luminescence intensity than Cu^{+}. In the evaluation of probe **1** under the same conditions, the solution containing the probe selectively changed from colorless to pink upon Cu^{+} addition, as detected by a naked eye (Figure 2). When irradiated at 365 nm, the blue luminescence of probe **1** became intense yellow upon addition of Cu^{+}, whereas addition of the other individual metal ions, including Cu^{2+}, produced no change in the solution luminescence color.

The solution color (daylight) and luminescence color changes (UV irradiation) of the probes detected upon Cu^{+} addition were recapitulated in UV−visible and fluorescence studies. Probe **2** in water showed strong, intermediate, or weak absorption in the 550−600 nm range upon addition of Cu^{+} (strong), Cu^{2+}/Hg^{2+} (intermediate), or Ag^{+} (weak) (Figure S4A). With probe **3**, adding Cu^{+} and Cu^{2+} to the solution resulted in strong and weak absorptions in the 530−550 nm range, respectively (Figure S4B). Thus, probes **2** and **3** showed moderate selectivity for Cu^{+} detection. Next, we found that the optimal excitation wavelengths for the fluorescence study were 520 and 460 nm for probes **2** and **3**, respectively (Figure S5). Upon excitation at those individual wavelengths, these probes showed intense fluorescence emission in the 550−600 nm range in the presence of Cu^{+} (Figure S4C,D). The addition of Hg^{2+} or Au^{3+} to the probe solutions showed slight increases in fluorescence intensity, indicating that these probes are suboptimal for selectively detecting Cu^{+} in water. On the other hand, probe **1** provided high selectivity for Cu^{+} detection. Upon the addition of Cu^{+}, this probe showed a strong absorption peak at 553 nm in the UV−visible spectrum and produced a strong fluorescence emission at 573 nm (I_{573}) upon excitation at 520 nm (Figure 2). Additions of the other metal ions to the probe solution produced only minor effects on both the absorption and fluorescence spectra of probe **1**.

The fluorescence emission of probe **1** was further studied by using different Cu(I) salts (CuCl, CuBr, and CuI). Only the addition of CuI to the probe led to a strong fluorescence intensity (Figure S6). Cu(I) tends to spontaneously oxidize to Cu(II) in solution and thus the oxidized Cu species needs to return back to Cu(I) for sensing of this metal ion, which was attained by iodide (I^{-}), a reducing agent, in this experiment.[40] The addition of NaI to the probe failed to induce fluorescence emission, indicating that I^{-} is unlikely to be responsible for the fluorescence emission observed here. The probe also showed little fluorescence emission in the presence of other reducing substances (Fe^{2+}, dithiothreitol, and cysteine (Cys)) or protein (bovine serum albumin) (Figure S6C). Thus, the response of the probe to Cu(I) is not ascribed to the reducing power of this metal ion. The probes (**1**−**3**) were further investigated by adding Cu^{+} in the presence of another metal ion, which allowed us to determine how another metal ion interferes with the detection of Cu^{+}. As expected, the ability of probe **2** to detect Cu^{+} tended to be strongly affected by the presence of another metal ion (Ag^{+} or Au^{3+}) (Figure S7). A similar result was observed with probe **3**; its ability to detect Cu^{+} was severely hindered by the presence of Hg^{2+}, Au^{3+}, or Ru^{3+}. In contrast, probe **1** did not suffer such interference from the nontarget metal ions (Figure 2D), indicating that probe **1** is superior to probes **2** and **3** in terms of selectively detecting Cu^{+} in an aqueous solution.

Cu^{+}-Sensing Capability of Probes 1−3. The changes in solution color and UV−visible and fluorescence spectra upon the addition of Cu^{+} likely reflect the binding of this metal ion

https://doi.org/10.1021/acssensors.3c02496
ACS Sens. 2024, 9, 1419−1427

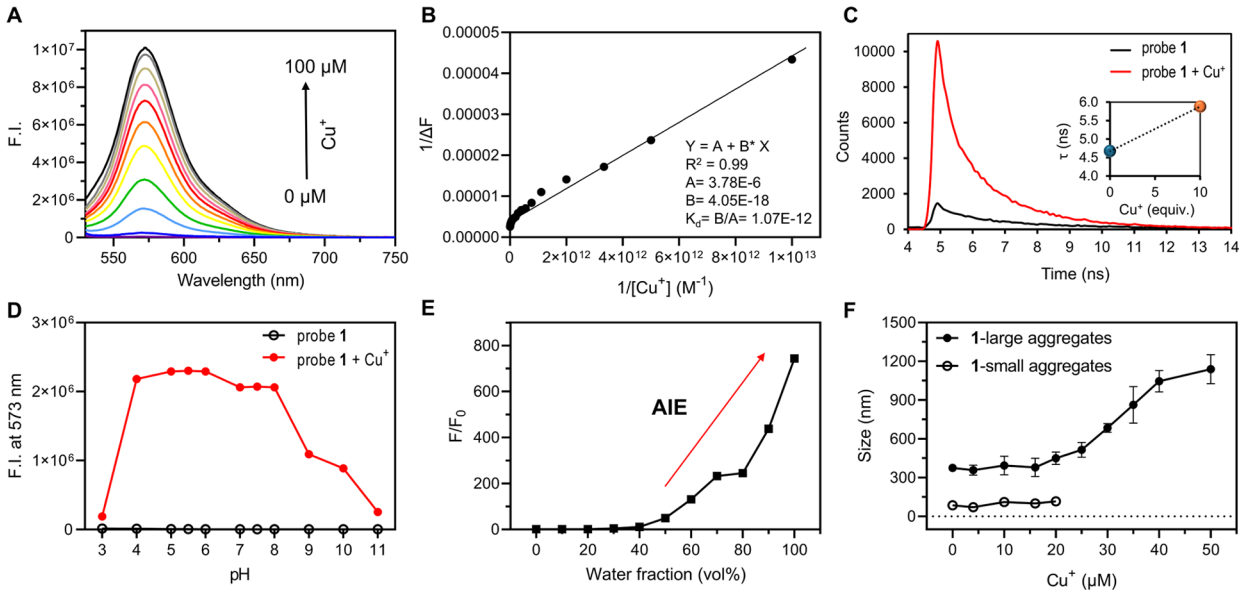

Figure 3. (A) Fluorescence titration of probe **1** (10 μM) with Cu^+ in water. The metal ion was used in the range of 0−100 μM, and the probe was excited at 520 nm. (B) Benesi−Hildebrand plot used for K_d determination, obtained from the titration data of probe **1** with Cu^+ (0, 0.1, 0.2, 0.3, 0.5, 0.9, 1.3, 1.8, 2.5, 3.5, 5.0, 7.0, 10.0, 15.0, 20.0, 30.0, 40.0, 60.0, 80.0, 100.0, 150.0, 200.0, 400.0, 600.0, 800.0 pM) in the presence of thiourea (100 mM). (C) Fluorescence decay profiles of probe **1** in water in the presence (red) and absence of Cu^+ (10 equiv; black). The inset shows a change in the excited state lifetime (τ) of the probe upon addition of the metal ion. (D) Changes in the fluorescence intensity (I_{573}) of probe **1** (10 μM) with pH variation in the absence and presence of Cu^+ (100 μM) in the phosphate-buffered saline (PBS). Excitation wavelength: 520 nm. (E) Changes in the fluorescence intensity ratio (F/F_0) of probe **1** with increasing water content in dimethylsulfoxide (DMSO). F_0 and F are the fluorescence intensities of the probe at 575 nm in the absence and presence of Cu^+ (100 μM), respectively. Excitation wavelength: 520 nm. (F) Changes in aggregate size displayed by probe **1** (10 μM) as the amount of Cu^+ increased from 0 to 50 μM. The probe formed both small and large aggregates in the presence of less than 25 μM Cu^+. The data are shown as the mean ± SD (n = 3).

to the individual probes (**1**−**3**). To find the binding stoichiometry between each probe and the metal ion, we mixed different molar ratios of probes **1** and **2** with Cu^+ in water and measured the fluorescence intensities at 573 nm (I_{573}) (Figure S8). The resulting Job plots show intersections of two lines at the x-axis values of 0.67 and 0.68 for probes **1** and **2**, respectively,[41] indicating that these probes bind Cu^+ in a ratio of 1:2. We could not obtain meaningful data for probe **3**, probably due to weak binding with this metal ion. Next, we carried out fluorescence titration of the probes with Cu^+. The fluorescence intensity (I_{573}) of probe **2** (10 μM) increased as the Cu^+ concentration increased up to 2 equiv (20 μM) relative to the probe (Figure S9B). No additional increase in fluorescence intensity was observed with the addition of more Cu^+. At this saturation point, a large increase (284-fold) in fluorescence intensity of the probe was observed, along with an increased quantum yield (ϕ) from 0.048 to 0.57. Probe **3** was similar to probe **2** in that the fluorescence intensity (I_{529}) increased with [Cu^+], but it increased more gradually than that of probe **2** (Figure S9C). In addition, the fluorescence intensity of this probe was not saturated at 2 equiv of Cu^+; instead, it continued to increase up to the addition of 5 equiv of Cu^+. The addition of 5 equiv of Cu^+ to the probe solution resulted in a 10-fold enhancement in the fluorescence intensity (I_{529}) relative to that observed in the absence of the metal ion. The comparison of those two probes indicates that probe **3** is less sensitive than probe **2** in detecting Cu^+ using fluorescence emission intensity. This is likely correlated with weaker binding between Cu^+ and probe **3** than between Cu^+ and probe **2**. As calculated from the fluorescence titration data, the LODs of probes **2** and **3** were 1.3 and 5.3 μM, respectively (Figure S9E,F).

When probe **1** was subjected to titration of the fluorescence produced with Cu^+, its fluorescence intensity at 573 nm (I_{573}) increased continuously up to the addition of 10 equiv of Cu^+ (Figure 3A). This behavior is similar to that of probe **3**, but the fluorescence emission enhancement obtained from probe **1** was 292-fold, significantly higher than that of probe **3**. The LOD of probe **1** for Cu^+ detection was calculated to be 20 nM, significantly better than those of both probe **3** (5.3 μM) and probe **2** (1.3 μM) (Figure S9). The K_d of probe **1** for Cu^+ binding was measured using thiourea as a competitive ligand in water, giving 1.1×10^{-12} M (Figure 3B).[34,42] The LOD and K_d obtained for probe **1** were one of the best of all previously reported probes for Cu^+ detection (Table S1), indicating its promise for sensitively detecting Cu^+. Of note, quantum yield of probe **1** could not be correctly calculated due to the formation of large aggregates in water, resulting in substantial light scattering. Rather, the fluorescence emission intensities of probes **1** and **2** were compared to each other in the presence of 10 equiv. Cu^+, using rhodamine B (ϕ = 0.31) as a reference (Figure S11B). In the absence of Cu^+, these probes were little fluorescent (Figure S11A). Time-resolved fluorescence spectroscopy allowed us to find that the excited state lifetimes (τ) of probes **1** and **2** increased from 4.7 to 5.9 ns (probe **1**) and from 4.4 to 5.7 ns for probe **2** (Figures 3C and S12).[26]

The rhodamine hydrazide-based fluorophore is known to undergo protonation and subsequent opening of the spirolactam ring in acidic conditions, resulting in a large increase in fluorescent intensity at 550−590 nm.[43−45] Based on that, we investigated the performance of our rhodamine hydrazide-based probes for Cu^+ detection according to solution pH maintained by a PBS-buffered system. In the absence of Cu^+, as expected, the fluorescent intensity of probe

https://doi.org/10.1021/acssensors.3c02496
ACS Sens. 2024, 9, 1419−1427

1 at 575 nm (I_{575}) was relatively weak and varied little in the pH range of 5−11, but it tended to increase when the solution pH was less than 5 (Figure S13). This increase is likely due to the protonation of the carbonyl group under the conditions, resulting in the spirolactam ring cleavage.[46] In the presence of Cu^+, the probe showed high fluorescence intensity in the pH range 4−8, but the fluorescence emission weakened when the solution pH deviated from that optimal range (Figure 3D). This weakened fluorescence emission probably originates from either the protonation of the carbonyl group or association of OH^- with Cu^+, leading to the decreased binding of the metal ion to the probe. Thus, probe **1** effectively detected Cu^+ in a solution pH range of 4−8, potentiating its suitability for detecting Cu^+ in biological samples.

Cu^+ Sensing Mechanism of Probes 1−3. All of the results described above consistently indicate that probe **1** is superior to probes **2** and **3** in sensitively and selectively detecting Cu^+ in an aqueous solution. To explore the origin of this notable result, we first measured the color change of probe **1** (10 μM) when it was dissolved in various solvent systems and exposed to Cu^+ at 100 μM. When Cu^+ was added to those solutions, the probe dissolved in water, MeOH, or DCM showed a pink/purple color in daylight, as detected by the naked eye, and the other solutions were colorless (Figure S14A). Under irradiation of 365 nm, probe **1** dissolved in water, MeOH, or dichloromethane (DCM) showed yellow luminescence, with the most intense emission observed with water. Consistent with this result, the fluorescence intensity of the probe at 573 nm (I_{573}) increased most upon addition of Cu^+ when the probe was dissolved in water (Figure S14B,C).

We further investigated the fluorescence behavior of this probe by using a mixture of DMSO and water as a binary solvent. When the amount of water in DMSO increased to more than 40%, the fluorescence intensity of probe **1** at 573 nm increased dramatically in the presence of Cu^+, suggesting the AIE in 100% water (Figures 3E and S15). Similar increases in fluorescence intensity were observed for probes **2** and **3**, but the enhancement was substantially smaller than that displayed by probe **1** (Figure S16). To explore the role of AIE in Cu^+ sensing, we measured changes in particle size displayed by the probes (**1**−**3**) (10 μM) with an increasing water content in DMSO via dynamic light scattering (DLS). In the absence of the metal ion, the probes formed two sets of aggregates (small and large) at high water contents (60/80%) in DMSO (Figure S17). The two sets of aggregates formed by probe **1**, one at ∼85 nm and the other at ∼400 nm, showed little changes in the aggregate size upon addition of Cu^+ up to 2 equiv. (20 μM) (Figures 3F and S18). When the metal ion was further added to the probe up to 5 equiv, the DLS peak corresponding to the small particles disappeared, and the size of the large aggregates gradually increased from 400 nm to more than 1000 nm. Thus, probe aggregation appears to be intensified when more than 2 equiv of Cu^+ was added to the probe. A similar result was obtained for probe **3** (Figure S19B), which also formed small and large particles in water, with particle sizes of ∼50 and ∼ 250 nm, respectively. Unlike probes **1** and **3**, probe **2** showed no substantial variation in particle size as the amount of Cu^+ increased, and the small particles formed by this probe did not disappear upon the addition of up to 5 equiv of Cu^+ (Figure S19A). Probe aggregation was further supported by transmission electron microscopy (TEM). Consistent with the DLS results, TEM images of probes **1** and **3** show both small and large aggregates in the absence of Cu^+ (Figure S20A,C). Upon addition of 4 equiv of Cu^+ (40 μM), a substantial increase in particle size was observed as the probes formed large aggregates. In contrast, probe **2** showed a negligible increase in aggregate size upon addition of the metal ion (Figure S20B). Taken together, these results indicate that the AIE plays a key role for probe **1** in effective Cu^+ detection, although the substantial increase in the sizes of large aggregates was a common feature of both probes **1** and **3** upon addition of 5 equiv of Cu^+. In the case of probe **2**, the AIE cannot be expected as no size increase in the probe aggregates was observed upon the addition of Cu^+.

Molecular Interaction between the Probe and Cu^+. To find the metal binding site of probe **1**, we first obtained the ^{1}H NMR spectrum of the probe with increasing equiv of Cu^+. The individual NMR peaks of probe **1** were assigned based on 2D NMR spectra (^{1}H−^{1}H NOESY, COSY, and HSQC) (Figures S21−S23). As the amount of Cu^+ increased, the triazole C5-proton peaks (H_t) of probe **1** disappeared, indicating that the metal ion binds to the deprotonated C5 of the triazole ring (Figure S24). Some signals, such as H_d, H_f, and H_g, were shifted downfield, suggesting the coordination of Cu^+ to the carbonyl group on the lactam ring to facilitate the opening of the spirolactam ring. This binding is responsible for generating the pink color and strong fluorescence emission at 573 nm observed when this probe is exposed to Cu^+. We also observed gradual peak broadening of all proton signals as Cu^+ concentration increased, corroborating the finding of probe aggregation in water. When probes **2** and **3** were studied under the same conditions, similar results were obtained (Figures S25 and S26). These results were expected because all of the tested probes (**1**−**3**) contain an acidic triazole C5−H and lactam carbonyl group for Cu^+ binding. To further investigate the molecular interaction between each probe and Cu^+, we used density functional theory (DFT) calculations at the B3LYP/6-31G* level. The coordination of two Cu^+ ions to probe **1** was calculated to induce a substantial conformational change, reminiscent of the induced fit of an enzyme−substrate interaction (Figure S27A). The calculations show that the probe can bind two Cu^+ ions, which is consistent with the 1:2 stoichiometry of the [probe **1**+ Cu^+] complex obtained from the Job plot. The first binding site of the probe comprises three atoms: triazole N, triazine N, and the rhodamine carbonyl group. Binding of Cu^+ to this binding site is responsible for the fluorescence emission of the probe upon the addition of Cu^+. The second binding site is in the linker region between the maltose hydrophilic group and the triazine core and also comprises three atoms: triazole C5, triazole N, and maltose 2-OH. The Cu^+ binding site of probe **2** was the same as for probe **1**, as expected because the probes have the same structure except for the length of the lipophilic alkyl chain (Figure S28A). For probe **3**, we found only a single binding site comprising triazole N, triazine N, and the rhodamine carbonyl group, similar to the first Cu^+ binding site of probes **1** and **2** (Figure S29A). This calculation result is consistent with the color change and fluorescence emission described above for this probe upon Cu^+ binding.

The DFT calculations also give information about the energy levels and electron distribution of the frontier orbitals (the highest occupied molecular orbital (HOMO) and the lowest unoccupied molecular orbital (LUMO)). The calculations show that the HOMO and LUMO of probe **1** are located in different regions of the rhodamine unit: the dibenzopyran ring for the HOMO and the benzolactam ring

https://doi.org/10.1021/acssensors.3c02496
ACS Sens. 2024, 9, 1419−1427

Table 1. Photo-Physical Properties and the Limits of Detection (LODs) of Probes 1−3 in the Presence of Cu^{+a}

	UV−vis., λ_{max} (nm)	Flu., λ_{em} (nm)	LOD (Flu.) (μM)	energy levels of the probes (eV)			energy levels of the [probe +2Cu^+] - closed form (eV)			energy levels of the [probe +2Cu^+] - open form (eV)		
probe	with Cu^+			HOMO	LUMO	E gap	HOMO	LUMO	E gap	HOMO	LUMO	E gap
1	553	573	0.02	−5.30	−1.12	4.18	−8.36	−6.18	2.18	−8.35	−6.19	2.16
2	552	573	1.3	−5.19	−1.20	3.99	−8.23	−6.17	2.06	−8.21	−6.18	2.03
3	530	529	5.3	−5.05	−0.90	4.15	−6.99	−3.60	3.39	−6.94	−4.88	2.06

[a]Along with energy levels of the frontier orbitals (HOMO and LUMO) of the probes and their Cu^+ complexes in the closed and open forms, as determined by DFT calculations.

for the LUMO (Figure S27B). When two Cu^+ ions bind to the probe, the HOMO electron density is the same as that of free probe **1**, but the LUMO electron density moves from the benzolactam ring of the fluorophore to the first Cu^+-binding site of the probe (Figure S27B). Opening of the benzolactam ring induced by Cu^+ binding results in little change in the electronic distributions of HOMO and LUMO compared to those of the probe complexed with two copper ions in a ring-closed form. Upon binding of two copper ions, the HOMO−LUMO energy gap of the probe was reduced from 4.2 to 2.2 eV. We also calculated the HOMO and LUMO energy levels of the [probe-Cu^+] complex following spirolactam ring-opening induced by Cu^+ binding. We found a small HOMO−LUMO energy gap for the ring-opened [probe-Cu^+] complex, which explains the absorption peak at 553 nm (A_{553}) and fluorescence emission peak at 573 nm (I_{573}) upon Cu^+ addition. A similar trend was observed for probe **2**, which showed HOMO and LUMO electron density mainly in the dibenzopyran and benzolactam rings of the fluorophore, respectively (Figure S28B). Binding between two Cu^+ ions and the probe and subsequent ring opening produce little change in the location of the HOMO electron density, but the LUMO electron density shifted to the first metal binding site.

The HOMO−LUMO energy gap was decreased from 3.99 to 2.06 eV upon binding of two copper(I) ions. Following the opening of the benzolactam ring, the HOMO−LUMO energy gap was further reduced to 2.03 eV (Figure S28B). The metal binding to probe **3** also decreases the HOMO−LUMO energy gap from 4.15 to 3.39 eV (Figure S29B). The ring-opened complex between the probe and Cu^+ further reduced the HOMO−LUMO energy gap to 2.06 eV. The photophysical properties and HOMO−LUMO energy levels of probes **1**−**3** are summarized in Table 1. Based on the fluorescence, NMR, DLS, and DFT results, we propose a Cu^+-sensing mechanism for probe **1**, as shown in Figure 4. Binding between two copper(I) ions and the probe triggers opening of the spirolactam ring of the rhodamine unit, resulting in the aggregation of probe−metal complexes for fluorescence emission enhancement. The Cu^+-binding-induced bond cleavage and resulting large aggregate formation indicate that the Cu^+ sensing of the probe is irreversible (activity-based).

Application of Probe 1 for Cell Imaging. We explored the potential of activity-based probe **1** to detect the Cu(I) level within living cells. First, we used human skin cancer cells (SK-MEL-28) and human breast cancer cells (MDA-MB-231) to measure Cu(I) levels in cytoplasm. When treated with probe **1** (5 μM), both cell lines displayed "TURN-ON" fluorescence emissions, indicating that the probe can penetrate cell membranes (Figure S30). These cancer cells showed little fluorescence emission in the absence of the probe. The pretreatment of those cancer cells with $CuCl_2$ (50 μM) increased the fluorescence intensity compared to the control

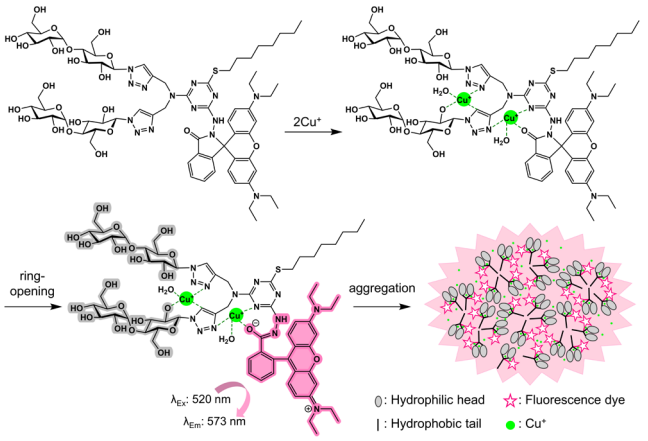

Figure 4. Proposed Cu^+-sensing mechanism of probe **1**. The probe contains two binding sites for Cu^+. Cu^+ binding to the carbonyl group of the rhodamine fluorophore induces the spirolactam ring to open, resulting in an intense fluorescence emission at 573 nm followed by the aggregation of the probe−metal ion complex. This aggregation is facilitated by the presence of a hydrophobic long alkyl chain in the probe, resulting in a large enhancement in the fluorescence emission.

cells that received no pretreatment, as a consequence of the increased cellular levels of Cu(I). This result encouraged us to evaluate the probe in terms of ability to differentiate cancer cells from normal cells via Cu(I) level detection. Cancer cells tend to contain more Cu(I) levels than normal cells to accommodate their high cell proliferation and division activity.[47−52] When human lung cancer (A549) and normal cells (HEL299) were treated with the probe, we found that A549 cancer cells exhibited a higher fluorescence intensity than normal HEL299 cells (Figure 5). This result indicates that probe **1** holds potential in the detection of human lung cancer. The pretreatment of these lung cells (HEL299 and A549) with $CuCl_2$ resulted in further increases in fluorescence intensity, as observed with the skin and breast cancer cells above. The probe exhibited no toxicity up to 50 μM in all these cell lines (A549, HEL299, SK-MEL-28, and MDA-MB-231 cells) (Figure S31).

CONCLUSIONS

Our new fluorescent probe **1** is highly effective for sensing Cu^+ in an aqueous environment. The probe has a triazine core decorated with three functional units: a lipophilic alkyl chain (octyl), a fluorophore (rhodamine B hydrazine), and a hydrophilic carbohydrate (maltose). The individual units play distinct roles in Cu^+ sensing. Upon binding two equiv of Cu^+ to the probe, the spirolactam ring of the rhodamine B-based fluorophore opens to generate a pink color, and the lipophilic octyl chain facilitates aggregation of [probe **1**-2Cu^+] complexes to induce AIE and ensure strong fluorescence

https://doi.org/10.1021/acssensors.3c02496
ACS Sens. 2024, 9, 1419−1427

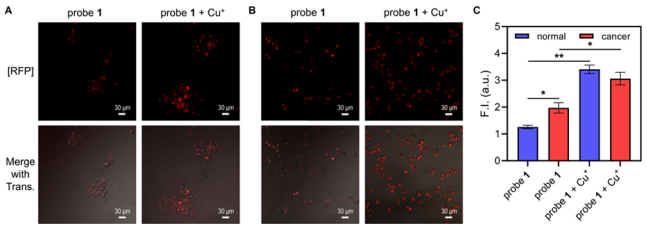

Figure 5. (A,B) (*top*) Confocal fluorescence images of HEL299 cells (human lung normal cells) (A) and A549 cells (human lung cancer cells) (B) using the red channel and (*bottom*) images merged with corresponding bright-field transmission images. The individual cancer cell lines were incubated with probe **1** (*left*) or with probe **1** and $CuCl_2$ (*right*). The cells were pretreated with 50 μM $CuCl_2$ for 6 h to allow Cu^{2+} uptake and then incubated with 5 μM probe **1** for 30 min at 37 °C. After uptake, copper ion is present in the cell interior as Cu^+ due to reduction by transmembrane protein. (C) Analyses on fluorescence intensity via ImageJ for the confocal images of HEL299 and A549 cells.[53] The data are shown as a mean ± SD (n = 3). P values were calculated by the Student's two-sided t test (*p < 0.05, **p < 0.01).

emissions. The hydrophilic maltose units make the probe water-soluble, which allowed us to evaluate the probe's ability to sense Cu^+ in aqueous solutions, including living cells. In addition, this hydrophilic group participates in Cu^+ binding in collaboration with two neighboring triazole rings. The central triazine ring used to bring the three functional units (alkyl chain, rhodamine B hydrazine, and triazole-maltose conjugate) into a single molecular probe is also involved in binding copper(I). Probe **2**, which has a short ethyl chain instead of a long octyl chain, failed to produce AIE, although it did show the ability to bind two copper(I) ions and produce notable changes in both the solution color and fluorescence intensity. As a result, probe **2** was unable to respond to the addition of more than 2 equiv of Cu^+. Probe **1** was superior to probe **2** in sensitively detecting Cu^+ in an aqueous solution because it showed both strong Cu^+ binding and AIE. Probe **3**, which has an octyl chain, displayed only weak/little AIE in its fluorescence emissions upon Cu^+ binding. In addition, it contains a single binding site for copper(I) ions, which dramatically reduces its binding affinity to Cu^+. Consequently, this probe was poor at effectively detecting Cu^+ in aqueous media. The LOD (20 nM) and K_d (1.1×10^{-12} M) calculated for probe **1** were significantly better than the other values reported to date. Such ultrahigh sensitivity and strong metal ion binding can be achieved through the multiple favorable properties of this probe, including its AIE effect and the presence of two metal ion-binding sites. In addition, previously reported probes were shown to be effective at Cu^+ sensing up to 1 equiv. addition of the metal ion due to their 1:1 binding stoichiometry and the absence of AIE. In contrast, probe **1** successfully detected Cu^+ in a wider range of concentrations (up to 10 equiv) than previously reported probes. Furthermore, this activity-based probe effectively detected different Cu(I) levels between human lung cancer cells and normal cells. Our results not only provide an excellent showcase of chemical sensor development for Cu^+ detection but also introduce a probe with potential for studying copper biology, cellular imaging, and early disease detection.

METHODS

LOD and K_d Calculations. The LOD was determined using fluorescence titration data for each probe with Cu^+ and the eq $3\sigma/S$, where σ and S represent the standard deviation of the blank measurement and the slope of the linear fit between the fluorescence intensity of the probe (**1**, **2**, or **3**) and $[Cu^+]$, respectively. The K_d was determined using the equation $(F - F_{min})/(F_{max} - F_{min}) = [Cu^+]/(K_d + [Cu^+])$, where F is the fluorescence emission intensity in the presence of Cu^+, F_{max} is the maximum fluorescence intensity of $[probe\text{-}Cu^+]$ complex, and F_{min} is the fluorescence intensity of free probe **1**.

Theoretical Calculations. Gradient-correlated DFT calculations using Becke's three-parameter exchange functional[54] and the Lee–Yang–Parr (B3LYP) exchange-correlation function[55] with 6-31G* basis sets for C, H, N, and O were used to obtain the energy-minimized structures of the new probes (**1**–**3**) and their Cu^+ complexes. The calculations were carried out under vacuum to maintain simplicity. One or two H_2O molecules were added to allow Cu^+ binding. The verification of all stationary points as minima was achieved using Hessian and harmonic frequency analyses.[56,57]

Live Cell Imaging. HEL299, A549, SK-MEL-28, and MDA-MB-231 cells were obtained from the Korean Cell Line Bank and grown in a minimum essential medium supplemented with 10% fetal bovine serum (FBS), 100 IU/mL penicillin, and 100 μg/mL streptomycin. Cells were maintained in a humidified incubator at 37 °C with 5% CO_2. The day before probe treatment, 3×10^5 cells were seeded on the 13 mm glass bottom of a 35-mm confocal dish and grown for 24 h to 70–80% confluence. Experiments were performed in triplicate in FBS and an antibiotic-free medium as follows. The three types of cancer cells were incubated with $CuCl_2$ (50 μM) at 37 °C with 5% CO_2 for 6 h, followed by two washes with 1× phosphate-buffered saline (PBS) (pH 7.4). The cells were further incubated with probe **1** (5 μM) for 30 min under the same conditions and then washed three times with 1× PBS. Confocal microscopy images were obtained with a K1-Fluo confocal laser scanning microscope (Nanoscope Systems, Daejeon, Korea) with a 20× oil immersion objective lens. Bright-field images after treatment with probe **1** and $CuCl_2$ indicated that the cells were viable throughout the experiment. In these human cell lines (HEL299, A549, SK-MEL-28, and MDA-MB-231 cells), probe **1** was permissive and responsive to changes in the intracellular Cu(I) level within living cells.

Cytotoxicity Test. The cytotoxicity of probe **1** was determined using a water-soluble tetrazolium salt (WST)-1 cell proliferation reagent purchased from Sigma-Aldrich. HEL299, A549, SK-MEL-28, and MDA-MB-231 cells were cultured in a 96-well plate in a CO_2 incubator for 24 h at 37 °C. Then, the media were replaced with fresh media containing different concentrations of probe **1**. After 3 h, the cells were washed with Dulbecco's PBS and incubated with WST-1 solution for 2 h. Absorption values at 480 and 660 nm were determined by using a microplate reader (BioTek Instrument Inc., USA).

ASSOCIATED CONTENT

Supporting Information

The Supporting Information is available free of charge at https://pubs.acs.org/doi/10.1021/acssensors.3c02496.

UV–visible and Fluorescence spectra, Job plot, DLS data, TEM image, DFT calculations, cell imaging, synthetic protocols for the probes and ^1H, ^{13}C NMR data (PDF)

AUTHOR INFORMATION

Corresponding Authors

Gi Hun Seong − *Department of Bionano Engineering, Hanyang University, Ansan 155-88, Republic of Korea;* orcid.org/0000-0003-4688-713X; Email: ghseong@hanyang.ac.kr

Pil Seok Chae − *Department of Bionano Engineering, Hanyang University, Ansan 155-88, Republic of Korea;*

https://doi.org/10.1021/acssensors.3c02496
ACS Sens. 2024, 9, 1419–1427

orcid.org/0000-0003-1799-3304; Email: pchae@hanyang.ac.kr

Authors

Eunhye Jeong − *Department of Bionano Engineering, Hanyang University, Ansan 155-88, Republic of Korea;* orcid.org/0000-0003-2899-795X

Chang Hyeon Ha − *Department of Bionano Engineering, Hanyang University, Ansan 155-88, Republic of Korea*

Ashwani Kumar − *Department of Bionano Engineering, Hanyang University, Ansan 155-88, Republic of Korea*

Won Hur − *Department of Bionano Engineering, Hanyang University, Ansan 155-88, Republic of Korea;* orcid.org/0000-0002-4092-0165

Complete contact information is available at: https://pubs.acs.org/10.1021/acssensors.3c02496

Author Contributions

P.S.C. and E.J. designed the new probes. E.J. synthesized the probes. C.H.H., A.K., and W.H. designed and performed the research and interpreted the data. P.S.C., G.H.S., and A.K. contributed to experimental design and data interpretation. P.S.C. and E.J. wrote the manuscript, with oversight from all the other authors.

Funding

This work was supported by the National Research Foundation of Korea (NRF) (2018R1A6A1A03024231 to P.S.C.).

Notes

The authors declare the following competing financial interest(s): Pil Seok Chae and Eunhye Jeong are inventors on a patent application that covers the fluorescent probes.

REFERENCES

(1) Linder, M. C.; Hazegh-Azam, M. Copper biochemistry and molecular biology. *Am. J. Clin. Nutr.* **1996**, *63* (5), S797−S811.
(2) Schieber, M.; Chandel, N. S. ROS function in redox signaling and oxidative stress. *Current biology* **2014**, *24* (10), R453−R462.
(3) Valentine, J. S.; Hart, P. J. Misfolded CuZnSOD and amyotrophic lateral sclerosis. *Proc. Natl. Acad. Sci. U. S. A.* **2003**, *100* (7), 3617−3622.
(4) Bruijn, L. I.; Miller, T. M.; Cleveland, D. W. Unraveling the mechanisms involved in motor neuron degeneration in ALS. *Annu. Rev. Neurosci.* **2004**, *27*, 723−749.
(5) Barnham, K. J.; Masters, C. L.; Bush, A. I. Neurodegenerative diseases and oxidative stress. *Nat. Rev. Drug Discovery* **2004**, *3* (3), 205−214.
(6) Brown, D. R.; Kozlowski, H. Biological inorganic and bioinorganic chemistry of neurodegeneration based on prion and Alzheimer diseases. *Dalton Transactions* **2004**, *13*, 1907−1917.
(7) Gupte, A.; Mumper, R. J. Elevated copper and oxidative stress in cancer cells as a target for cancer treatment. *Cancer treatment reviews* **2009**, *35* (1), 32−46.
(8) Waggoner, D. J.; Bartnikas, T. B.; Gitlin, J. D. The role of copper in neurodegenerative disease. *Neurobiology of disease* **1999**, *6* (4), 221−230.
(9) Strausak, D.; Mercer, J. F.; Dieter, H. H.; Stremmel, W.; Multhaup, G. Copper in disorders with neurological symptoms: Alzheimer's, Menkes, and Wilson diseases. *Brain research bulletin* **2001**, *55* (2), 175−185.
(10) Peña, M. M.; Lee, J.; Thiele, D. J. A delicate balance: homeostatic control of copper uptake and distribution. *Journal of nutrition* **1999**, *129* (7), 1251−1260.
(11) Puig, S.; Thiele, D. J. Molecular mechanisms of copper uptake and distribution. *Curr. Opin. Chem. Biol.* **2002**, *6* (2), 171−180.
(12) Shanbhag, V. C.; Gudekar, N.; Jasmer, K.; Papageorgiou, C.; Singh, K.; Petris, M. J. Copper metabolism as a unique vulnerability in cancer. *Biochimica et Biophysica Acta (BBA)-Molecular Cell Research* **2021**, *1868* (2), 118893.
(13) Sun, T.; Zhang, G.; Guo, Z.; Chen, Q.; Zhang, Y.; Chu, Y.; Guo, Q.; Li, C.; Zhou, W.; Zhang, Y. Co-delivery of Cu (I) chelator and chemotherapeutics as a new strategy for tumor theranostic. *J. Controlled Release* **2020**, *321*, 483−496.
(14) De Silva, A. P.; Gunaratne, H. N.; Gunnlaugsson, T.; Huxley, A. J.; McCoy, C. P.; Rademacher, J. T.; Rice, T. E. Signaling recognition events with fluorescent sensors and switches. *Chem. Rev.* **1997**, *97* (5), 1515−1566.
(15) Aragay, G.; Pons, J.; Merkoçi, A. Recent trends in macro-, micro-, and nanomaterial-based tools and strategies for heavy-metal detection. *Chem. Rev.* **2011**, *111* (5), 3433−3458.
(16) Quang, D. T.; Kim, J. S. Fluoro-and chromogenic chemodosimeters for heavy metal ion detection in solution and biospecimens. *Chem. Rev.* **2010**, *110* (10), 6280−6301.
(17) Wang, P.; Meng, F.; Su, H.; Liu, L.; Khan, M. A.; Li, H. A highly selective "turn-on" water-soluble fluorescent sensor for gallium ion detection. *RSC Adv.* **2021**, *11* (32), 19747−19754.
(18) Teng, M.; Zhou, Z.; Qin, Y.; Zhao, Y.; Zhao, C.; Cao, J. A water-soluble fluorescence sensor with high specificity for detecting hydrazine in river water detection and A549 cell imaging. *Sens. Actuators, B* **2020**, *311*, No. 127914.
(19) Yun, D.; Chae, J. B.; So, H.; Lee, H.; Kim, K.-T.; Kim, C. Sensing of zinc ions and sulfide using a highly practical and water-soluble fluorescent sensor: applications in test kits and zebrafish. *New J. Chem.* **2020**, *44* (2), 442−449.
(20) Hu, F.; Xu, S.; Liu, B. Photosensitizers with aggregation-induced emission: materials and biomedical applications. *Adv. Mater.* **2018**, *30* (45), No. 1801350.
(21) Patil, S.; Pandey, S.; Singh, A.; Radhakrishna, M.; Basu, S. Hydrazide−hydrazone small molecules as AIEgens: Illuminating mitochondria in cancer cells. *Chemistry−A. European Journal* **2019**, *25* (35), 8229−8235.
(22) Huang, L.; Chen, F.; Xi, P.; Xie, G.; Li, Z.; Shi, Y.; Xu, M.; Liu, H.; Ma, Z.; Bai, D. A turn-on fluorescent chemosensor for Cu2+ in aqueous media and its application to bioimaging. *Dyes Pigm.* **2011**, *90* (3), 265−268.
(23) Wang, J.; Long, L.; Xie, D.; Song, X. Cu2+-selective "Off−On" chemsensor based on the rhodamine derivative bearing 8-hydroxyquinoline moiety and its application in live cell imaging. *Sens. Actuators, B* **2013**, *177*, 27−33.
(24) Ghosh, P.; Roy, P. Structure−metal ion selectivity of rhodamine-based chemosensors. *Chem. Commun.* **2023**, *59* (35), 5174−5200.
(25) Wang, Y.; Wang, X.; Ma, W.; Lu, R.; Zhou, W.; Gao, H. Recent developments in rhodamine-based chemosensors: A review of the years 2018−2022. *Chemosensors* **2022**, *10* (10), 399.
(26) Zeng, L.; Miller, E. W.; Pralle, A.; Isacoff, E. Y.; Chang, C. J. A selective turn-on fluorescent sensor for imaging copper in living cells. *J. Am. Chem. Soc.* **2006**, *128* (1), 10−11.
(27) Taki, M.; Iyoshi, S.; Ojida, A.; Hamachi, I.; Yamamoto, Y. Development of highly sensitive fluorescent probes for detection of intracellular copper (I) in living systems. *J. Am. Chem. Soc.* **2010**, *132* (17), 5938−5939.
(28) Park, S.; Kim, H.-J. Highly selective and sensitive fluorescence turn-on probe for a catalytic amount of Cu (I) ions in water through the click reaction. *Tetrahedron Lett.* **2012**, *53* (33), 4473−4475.
(29) Saha, T.; Sengupta, A.; Hazra, P.; Talukdar, P. In vitro sensing of Cu+ through a green fluorescence rise of pyranine. *Photochemical & Photobiological Sciences* **2014**, *13*, 1427−1433.
(30) Guo, J.; Yuan, H.; Chen, Y.; Chen, Z.; Zhao, M.; Zou, L.; Liu, Y.; Liu, Z.; Zhao, Q.; Guo, Z. A ratiometric fluorescent sensor for tracking Cu (I) fluctuation in endoplasmic reticulum. *Sci. China: Chem.* **2019**, *62*, 465−474.

(31) Qi, J.; Han, M. S.; Tung, C.-H. A benzothiazole alkyne fluorescent sensor for Cu detection in living cell. *Bioorganic & medicinal chemistry letters* **2012**, *22* (4), 1747−1749.
(32) Domaille, D. W.; Zeng, L.; Chang, C. J. Visualizing ascorbate-triggered release of labile copper within living cells using a ratiometric fluorescent sensor. *J. Am. Chem. Soc.* **2010**, *132* (4), 1194−1195.
(33) Lim, C. S.; Han, J. H.; Kim, C. W.; Kang, M. Y.; Kang, D. W.; Cho, B. R. A copper (I)-ion selective two-photon fluorescent probe for in vivo imaging. *Chem. Commun.* **2011**, *47* (25), 7146−7148.
(34) Cao, X.; Lin, W.; Wan, W. Development of a near-infrared fluorescent probe for imaging of endogenous Cu+ in live cells. *Chem. Commun.* **2012**, *48* (50), 6247−6249.
(35) Priessner, M.; Summers, P. A.; Lewis, B. W.; Sastre, M.; Ying, L.; Kuimova, M. K.; Vilar, R. Selective detection of Cu+ ions in live cells via fluorescence lifetime imaging microscopy. *Angew. Chem., Int. Ed.* **2021**, *60* (43), 23148−23153.
(36) Cody, J.; Fahrni, C. J. Fluorescence sensing based on cation-induced conformational switching: copper-selective modulation of the photoinduced intramolecular charge transfer of a donor−acceptor biphenyl fluorophore. *Tetrahedron* **2004**, *60* (49), 11099−11107.
(37) Yang, L.; McRae, R.; Henary, M. M.; Patel, R.; Lai, B.; Vogt, S.; Fahrni, C. J. Imaging of the intracellular topography of copper with a fluorescent sensor and by synchrotron x-ray fluorescence microscopy. *Proc. Natl. Acad. Sci. U. S. A.* **2005**, *102* (32), 11179−11184.
(38) Álvarez, C. M.; García-Escudero, L. A.; García-Rodríguez, R.; Miguel, D. Beyond click chemistry: spontaneous C-triazolyl transfer from copper to rhenium and transformation into mesoionic C-triazolylidene carbene. *Chem. Commun.* **2012**, *48* (57), 7209−7211.
(39) Straub, B. F. μ-Acetylide and μ-alkenylidene ligands in "click" triazole syntheses. *Chem. Commun.* **2007**, *37*, 3868−3870.
(40) Hsueh, N.-C.; Hsiao, Y.-T.; Chang, M.-Y. CuI mediated synthesis of sulfonyl dihydrofurans. *Tetrahedron* **2017**, *73* (30), 4398−4406.
(41) Senthilvelan, A.; Ho, I. T.; Chang, K. C.; Lee, G. H.; Liu, Y. H.; Chung, W. S. Cooperative Recognition of a Copper Cation and Anion by a Calix [4] arene Substituted at the Lower Rim by a β-Amino-α, β-Unsaturated Ketone. *Chemistry−A. European Journal* **2009**, *15* (25), 6152−6160.
(42) Dodani, S. C.; Domaille, D. W.; Nam, C. I.; Miller, E. W.; Finney, L. A.; Vogt, S.; Chang, C. J. Calcium-dependent copper redistributions in neuronal cells revealed by a fluorescent copper sensor and X-ray fluorescence microscopy. *Proc. Natl. Acad. Sci. U. S. A.* **2011**, *108* (15), 5980−5985.
(43) Zhang, Z.; Deng, C.; Meng, L.; Zheng, Y.; Yan, X. A rhodamine hydrazide-based fluorescent probe for sensitive and selective detection of hypochlorous acid and its application in living cells. *Analytical Methods* **2015**, *7* (1), 107−114.
(44) Tang, Z.; Ding, X.-L.; Liu, Y.; Zhao, Z.-M.; Zhao, B.-X. A new probe based on rhodamine B and benzothiazole hydrazine for sensing hypochlorite in living cells and real water samples. *RSC Adv.* **2015**, *5* (121), 99664−99668.
(45) Hosseinjani-Pirdehi, H.; Mahmoodi, N. O. A.; Taheri, A.; Asalemi, K. A. A.; Esmaeili, R. Selective immediate detection of Cu2+ by a pH-sensitive rhodamine-based fluorescence probe in breast cancer cell-line. *Spectrochim. Acta, Part A* **2020**, *229*, No. 117989.
(46) Kim, H. N.; Lee, M. H.; Kim, H. J.; Kim, J. S.; Yoon, J. A new trend in rhodamine-based chemosensors: application of spirolactam ring-opening to sensing ions. *Chem. Soc. Rev.* **2008**, *37* (8), 1465−1472.
(47) Vaidya, S.; Kamalakar, P. Copper and ceruloplasmin levels in serum of women with breast cancer. *Indian J. Med. Sci.* **1998**, *52* (5), 184−187.
(48) Sharma, K.; Mittal, D.; Kesarwani, R.; Kamboj, V. Diagnostic and prognostic significance of serum and tissue trace elements in breast malignancy. *Indian J. Med. Sci.* **1994**, *48* (10), 227−232.
(49) Mao, S.; Huang, S. Zinc and copper levels in bladder cancer: a systematic review and meta-analysis. *Biological trace element research* **2013**, *153*, 5−10.
(50) Baharvand, M.; Manifar, S.; Akkafan, R.; Mortazavi, H.; Sabour, S. Serum levels of ferritin, copper, and zinc in patients with oral cancer. *Biomed J.* **2014**, *37* (5), 331−336.
(51) Diez, M.; Arroyo, M.; Cerdan, F.; Munoz, M.; Martin, M.; Balibrea, J. Serum and tissue trace metal levels in lung cancer. *Oncology* **2004**, *46* (4), 230−234.
(52) Dragutinović, V. V.; Tatić, S. B.; Nikolić-Mandić, S. D.; Tripković, T. M.; Dunđerović, D. M.; Paunović, I. R. Copper as ancillary diagnostic tool in preoperative evaluation of possible papillary thyroid carcinoma in patients with benign thyroid disease. *Biological trace element research* **2014**, *160*, 311−315.
(53) Dong, S.; Cho, H. J.; Lee, Y. W.; Roman, M. Synthesis and cellular uptake of folic acid-conjugated cellulose nanocrystals for cancer targeting. *Biomacromolecules* **2014**, *15* (5), 1560−1567.
(54) Becke, A. D. Density-functional thermochemistry. I. The effect of the exchange-only gradient correction. *J. Chem. Phys.* **1992**, *96* (3), 2155−2160.
(55) Lee, C.; Yang, W.; Parr, R. G. Development of the Colle-Salvetti correlation-energy formula into a functional of the electron density. *Phys. Rev. B* **1988**, *37* (2), 785.
(56) Schmidt, M. W.; Baldridge, K. K.; Boatz, J. A.; Elbert, S. T.; Gordon, M. S.; Jensen, J. H.; Koseki, S.; Matsunaga, N.; Nguyen, K. A.; Su, S. General atomic and molecular electronic structure system. *J. Comput. Chem.* **1993**, *14* (11), 1347−1363.
(57) Huber, R. G.; Margreiter, M. A.; Fuchs, J. E.; von Grafenstein, S.; Tautermann, C. S.; Liedl, K. R.; Fox, T. Heteroaromatic π-stacking energy landscapes. *J. Chem. Inf. Model.* **2014**, *54* (5), 1371−1379.

https://doi.org/10.1021/acssensors.3c02496
ACS Sens. 2024, 9, 1419−1427